Biochemical Pharmacology 83 (2012) 1195–1207

Contents lists available at SciVerse ScienceDirect

Biochemical Pharmacology

journal homepage: www.elsevier.com/locate/biochempharm

Antiproliferative mechanisms of action of the flavin dehydrogenase inhibitors diphenylene iodonium and di-2-thienyliodonium based on molecular profiling of the NCI-60 human tumor cell panel

James H. Doroshow [a,b,*], Agnes Juhasz [a], Yun Ge [a], Susan Holbeck [b], Jiamo Lu [a], Smitha Antony [a], Yongzhong Wu [a], Guojian Jiang [a], Krishnendu Roy [b]

[a] Center for Cancer Research, National Cancer Institute, NIH, Building 37, 37 Convent Drive, Bethesda, MD 20892, USA
[b] Division of Cancer Treatment and Diagnosis, National Cancer Institute, NIH, Building 31, Room 3A-44, Bethesda, MD 20892, USA

ARTICLE INFO

Article history:
Received 5 October 2011
Accepted 17 January 2012
Available online 24 January 2012

Keywords:
Diphenylene iodonium
Dithienyliodonium
Reactive oxygen
Stat signaling
NADPH oxidase
NCI-60 tumor panel

ABSTRACT

Flavoprotein-dependent reactive oxygen species (ROS) play a critical role in cytokine-mediated signal transduction in normal tissues and tumor cells. The flavoenzyme inhibitors diphenylene iodonium (DPI) and di-2-thienyliodonium (DTI) have been used to inhibit membrane-bound, flavoprotein-containing NADPH oxidases, including epithelial and leukocyte NADPH oxidases (Nox1-5 and Duox 1 and 2). Recent evidence suggests that DPI can decrease tumor cell proliferation; however, the molecular mechanisms involved remain poorly defined. To explore the mechanisms underlying DPI- and DTI-related tumor cell growth delay, we examined growth inhibition patterns produced by both agents in the NCI-60 tumor panel, and determined expression levels of Nox gene family members across these cell lines. Possible molecular targets were predicted using the COMPARE program. DPI was more potent than DTI (GI_{50}: 10 nM versus 10 μM); DPI and DTI exposure produced unique patterns of growth inhibition when evaluated against the small molecule anticancer database of the National Cancer Institute. Growth inhibition profiling of DPI revealed a modest positive correlation with Nox1 levels; novel mechanisms of DPI and DTI action, including alterations in Stat, Erk1/2, and Akt pathways, were inferred by correlation with NCI-60 Affymetrix® array data. Exposure of HT-29 colon cancer cells, which express Nox1, to DPI and DTI confirmed their inhibitory effects on steady state ROS levels, and demonstrated decreased Stat, Erk1/2, and Akt signaling mediated by IL-4, IL-6, IL-13, and IL-22, possibly due to a concomitant increase in tumor cell phosphatase activity. These findings suggest that DPI and DTI may act therapeutically by altering ROS-related signal transduction.

Published by Elsevier Inc.

1. Introduction

Over the past decade, six epithelial NADPH oxidases (Noxs) distinct from the NADPH oxidase of leukocytes (Nox2) have been discovered; each demonstrates substantial homology to the leukocyte protein, but the epithelial enzymes have specific organ distributions and a variety of different physiological functions [1]. Reactive oxygen species (ROS) are generated by the epithelial Nox proteins in many tissue types during the course of growth factor- and cytokine-mediated signal transduction [2,3]. We recently demonstrated that Nox enzymes are distributed in a highly specific fashion in human tumors, and that Nox expression in tumor cells can be induced by pro-inflammatory cytokines [4,5]. These studies, as well as other investigations indicating that Nox-related ROS production plays an important role in tumor cell growth, adhesion, and angiogenesis [6,7], suggest that targeting ROS production by members of the Nox family or by other flavoproteins (including the mitochondrial electron transport chain) might be an attractive anticancer strategy.

Originally developed as anti-hyperglycemic agents based on their ability to inhibit gluconeogenesis through inhibition of mitochondrial complex I [8], diphenyleneiodonium (DPI) and di-2-thienyliodonium (DTI) have been utilized as inhibitors of the activities of a variety of different flavoproteins for more than 40 years [9,10] (Fig. 1). Following the initial demonstration of the

Abbreviations: ROS, reactive oxygen species; DPI, diphenyleneiodonium; DTI, di-2-thienyliodonium; NCI-60, National Cancer Institute panel of 60 human tumor cell lines; Nox, NADPH oxidase; Duox, dual oxidase.

* Corresponding author at: Division of Cancer Treatment and Diagnosis, National Cancer Institute, NIH, Building 31, Room 3A-44, 31 Center Drive, Bethesda, MD 20892, USA. Tel.: +1 301 496 4291; fax: +1 301 496 0826.
E-mail addresses: doroshoj@mail.nih.gov (J.H. Doroshow), juhasza@mail.nih.gov (A. Juhasz), Yun.Ge@fda.hhs.gov (Y. Ge), holbecks@mail.nih.gov (S. Holbeck), lujiamo@mail.nih.gov (J. Lu), antonys@mail.nih.gov (S. Antony), wuy@mail.nih.gov (Y. Wu), gjiang@mail.nih.gov (G. Jiang), royk@navmed.nci.nih.gov (K. Roy).

0006-2952/$ – see front matter. Published by Elsevier Inc.
doi:10.1016/j.bcp.2012.01.022

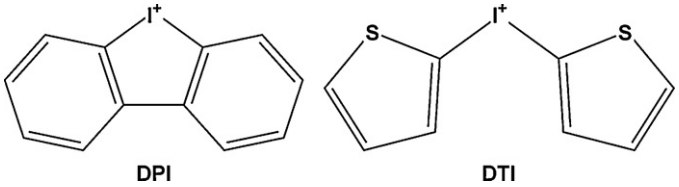

Fig. 1. Chemical structures of diphenyleneiodonium (DPI) and di-2-thienyliodonium (DTI).

capacity of these compounds to inhibit the production of ROS by Nox2 [11], through formation of a covalent complex with the flavin-containing component of the oxidase [12], iodonium compounds have been widely used to investigate the biochemical functions of flavin-dependent enzymes in vitro and in vivo [13,14].

DPI has routinely been employed in these investigations at concentrations $\geq$10 μM to inhibit Nox-dependent reactive oxygen production [15]. However, altering flavoprotein-related electron flow in cells at high DPI concentrations can actually induce, rather than inhibit, oxidative stress by blocking several components of the pentose phosphate pathway leading to diminished intracellular reduced glutathione pools with a subsequent decrease in the capacity to eliminate hydrogen and lipid peroxides [16]. Furthermore, a variety of other biochemical pathways are also inhibited by DPI, often at high concentrations, including alterations in non-flavin dehydrogenase-dependent cell systems (such as ion channels), by mechanisms that are poorly understood [13,17]. In light of these observations, it is not surprising that DPI possesses antitumor activity in vitro [18,19]. In the current study, we sought to develop a broader perspective regarding potential antiproliferative mechanisms of action for these two iodonium-class agents.

Initiated in the late 1980s, the National Cancer Institute 60 human tumor cell panel (NCI-60) has been extensively used to screen molecules for anticancer activity [20]. This panel contains nine different human tumor cell types, including leukemia, melanoma, prostate, breast, colon, central nervous system, ovary, kidney, and lung cancers. The cytostatic and cytotoxic profiles of small molecules are determined by sulphorhodamine B assays performed at five concentration levels of the agent under investigation. Because the cytostatic and cytotoxic patterns produced by the tested compounds across the panel may reflect similarities in biological properties and/or chemical structure, putative mechanisms have been inferred from the differential sensitivity and resistance patterns of cell lines after ranking and comparing the similarity of these profiles with those in the NCI Developmental Therapeutics Program database using the COMPARE algorithm [21]. COMPARE is an automated pattern-comparing tool that can directly import the screening data from the NCI-60 tumor panel to determine if a test drug has a similar cytostatic or/and cytotoxic pattern to an existing drug of known mechanism in the NCI database. Furthermore, COMPARE can serve as a search engine to explore molecular targets relevant to the cytostatic and cytotoxic action of compounds [20].

In this study, cytostatic and cytotoxic profiles for DPI and DTI, as well as Nox gene expression levels, were generated using the NCI-60 tumor cell line platform, and putative mechanisms of antiproliferative action and potential molecular targets for DPI and DTI were predicted by comparing the activity fingerprints of these agents to a database including small molecules with known mechanisms of action or a dataset including multiple Affymetrix® gene expression profiles, using the COMPARE program. We found that DPI and DTI produced unique patterns of cytostasis and cytotoxicity in the NCI-60 panel; while DPI is more potent (nM activity) than DTI, a more limited repertoire of molecular pathways appears to be involved in the antiproliferative effects of DTI. The expression level of only one member of the Nox family (Nox1) was related to growth inhibition by DPI, perhaps because of the relatively low level of expression of the entire Nox gene family across the NCI-60. Using the COMPARE algorithm, tumor cell functions predicted to be related to growth inhibition by DPI and DTI included modulation of Jak/Stat signaling, mitochondrial respiration, and cell cycle progression from G_1 to S phase. Because the effects of the iodonium analogs on mitochondrial respiration and cell cycle progression had previously been described, to qualify the predictions from our COMPARE evaluation, we directly examined whether DPI or DTI altered whole cell and mitochondrial reactive oxygen production, and whether changes in cellular ROS levels might affect cytokine signaling through the Jak/Stat, Erk1/2, and Akt pathways. We found that both agents produced substantial inhibitory effects on the activation of Stat, Erk1/2, and Akt proteins essential for cytokine-mediated tumor cell proliferation, and that changes in phosphorylation were associated with increases in tumor cell phosphatase activity. These findings suggest that DPI and DTI not only interfere with membrane oxidase functions, but interact across several distinct molecular pathways to produce a unique profile of antiproliferative activity.

2. Materials and methods

2.1. Reagents, cell culture, and drug sensitivity testing

Diphenylene iodonium (DPI; NSC 735294) was purchased from Sigma–Aldrich (St. Louis, MO); di-2-thienyliodonium (DTI; NSC 734426) was synthesized by the Developmental Therapeutics Program, Division of Cancer Treatment and Diagnosis of the National Cancer Institute, Bethesda, MD. DPI and DTI were prepared in dimethylsulfoxide (Sigma–Aldrich, St. Louis, MO) at their maximum soluble concentration. IL-4, IL-6, IL-13, and IL-22 were purchased from R&D Systems, Inc. (Minneapolis, MN, USA). The redox sensitive dyes CM-H_2-DCF-DA (catalog number C6827) and MitoSOX™ Red mitochondrial superoxide indicator (catalog number M36008) were both obtained from Life Technologies (Carlsbad, CA).

The standard operating procedures used for cell culture of the National Cancer Institute panel of 60 human tumor cell lines (NCI-60) and for drug sensitivity testing in these cell lines have been described previously [20,22,23]. All cultures were maintained at 37 °C in a humidified atmosphere of 5% CO_2 in air. Periodically, the cell lines were tested for Mycoplasma to ensure absence of contamination. The NCI-60 cancer cell lines were grown in RPMI 1640 medium supplemented with 5% fetal bovine serum and 2 mM L-glutamine (Lonza, Walkersville, MD). Cells were dispersed into a series of 96-well microtitre plates at an appropriate density and incubated for 1 day in the absence of drug; some of the plates are then processed to determine the density at time zero. After the initial 24 h drug-free period, serial 10-fold dilutions of DPI and DTI over a 5-log mol/L concentration range were added for 48 h of exposure. The protein content was determined by sulphorhodamine B staining after the cells were fixed in 10% trichloroacetic acid (TCA). The percentage growth inhibition was determined relative to cells without drug treatment and the time zero control. The use of the time zero control allows for the evaluation of cell kill as well as net growth inhibition. The GI_{50} is the log mol/L concentration yielding a growth percent of 50 (i.e., 50% growth inhibition). TGI, or total growth inhibition, is the log mol/L concentration yielding a growth percent of 0. Lethal concentration 50 (LC_{50}) is the log mol/L concentration yielding a growth percent of −50, or lethality in 50% of the starting cells. For purposes of illustration, cell lines with a mean GI_{50} and confidence intervals greater than the overall mean GI_{50} − 1 SD from all samples were deemed relatively sensitive

Table 1
Effect of DPI and DTI on the growth of sensitive and resistant tumor cell lines in the NCI-60 panel.

Tumor	Cell line	GI50		TGI		LC50	
		DPI	DTI	DPI	DTI	DPI	DTI
Sensitive cell lines (nM)							
Leukemia	CCRF-CEM	10	2.69×10^3	2.19×10^3	1.20×10^4	6.76×10^4	8.71×10^4
Leukemia	K-562	10	4.16×10^3	4.57×10^3	2.51×10^4	6.46×10^4	9.77×10^4
Leukemia	RPMI-8226	10	0.95×10^3	0.55×10^3	7.53×10^3	3.63×10^4	8.71×10^4
Leukemia	SR	10	2.82×10^3	10.72	5.62×10^3	4.68×10^3	1.91×10^4
NSCLC	NCI-H460	10	0.69×10^3	9.78×10^3	8.91 10^3	6.76×10^4	7.76×10^4
Colon	HCC-2998	95.5	4.89×10^3	1.23×10^4	1.86×10^4	4.07×10^4	5.13×10^4
CNS	SF-295	95.5	4.79×10^3	4.57×10^3	1.78×10^4	6.76×10^4	5.89×10^4
Melanoma	SK-MEL-5	10	0.912×10^3	3.39×10^3	2.88×10^3	3.24×10^4	7.76×10^4
Renal	CAKI-1	11.5	2.34×10^3	0.45×10^3	6.76×10^3	8.71×10^3	2.95×10^4
Resistant cell lines (nM)							
NSCLC	HOP-62	4.79×10^3	1.45×10^4	2.69×10^4	3.31×10^4	8.51×10^4	7.59×10^4
NSCLC	NCI-H226	7.76×10^3	1.51×10^4	3.63×10^4	3.09×10^4	9.12×10^4	6.31×10^4
Colon	KM12	3.47×10^3	2.95×10^3	2.88×10^4	1.12×10^4	9.12×10^4	8.51×10^4
Renal	SN12C	8.32×10^3	1.41×10^4	3.88×10^4	2.88×10^4	9.55×10^4	5.89×10^4
Renal	TK-10	5.25×10^3	1.86×10^4	4.57×10^4	4.27×10^4	1×10^5	8.13×10^4
Breast	MDA-MB-231	1.48×10^4	1.62×10^4	4.89×10^4	3.47×10^4	9.33×10^4	7.59×10^4
Breast	HS 578T	3.24×10^3	2.51×10^4	1×10^5	1×10^5	1×10^5	1×10^5

(Table 1), whereas those with mean GI_{50} and confidence intervals greater than the overall mean GI_{50} + 1 SD from all samples were deemed relatively resistant.

The COMPARE algorithm for pattern recognition and comparison used for NCI-60 drug screening dataset analysis has been described previously [21]. Using DPI and DTI as "seed" compounds, the growth inhibition and cytotoxicity patterns across the NCI-60 were compared to those of agents in the NCI's database of compounds. The results were quantitated as a Pearson correlation coefficient (PCC), with the high-ranking compounds suggesting a related mechanism of action to that of the seed compound [21]. Because the NCI-60 cell line database also includes an extensive amount of molecular characterization data for the cells (RNA, miRNA, and protein expression, mutation, SNP, and DNA methylation frequency), the COMPARE algorithm was utilized to correlate patterns of gene expression with growth inhibition by DPI and DTI. COMPARE was also used to correlate our RT-PCR measurements with the tens of thousands of molecules that have previously been tested in the NCI-60 [20].

HT-29 and HCT-116 human colon cancer cells that were used for Western analysis and/or phosphatase assays were obtained from the American Type Culture Collection (ATCC, Manassas, VA) and were grown as previously described [4]. CCD 841 CoN normal human colon epithelial cells (ATCC catalog number CRL-1790) were also obtained from the American Type Culture Collection and were propagated in Eagle's Minimum Essential Medium and 10% FBS. Determination of the concentrations of DPI and DTI that produced a 50% inhibition of growth in CCD 841 cells (IC_{50}) was performed by counting cells utilizing a Cellometer Auto T4 Cell Counter (Nexcelom Bioscience LLC, Lawrence, MA).

2.2. RNA isolation and reverse transcription

RNA from cell lines was isolated using an RNeasy Mini Kit (Qiagen, Valencia, CA). Genomic DNA contamination was removed with DNase I treatment (Life Technologies [Ambion], Carlsbad, CA, USA). Samples were purified on the mini columns of the RNeasy Mini Kit. Integrity of the RNA was tested using an Agilent Bioanalyzer 2100 (Agilent Inc., Palo Alto, CA). The RNA concentration and A_{260}/A_{280} ratio were determined by NanoDrop (ThermoFisher, Wilmington, DE, USA). cDNA was prepared from 3 μg of RNA using MMLV reverse transcriptase enzyme and random hexamers as primers according to the manufacturer's instructions (Life Technologies, Carlsbad, CA), and stored at −20 °C until used. Real-time PCR was used to measure the level of gene expression. One μl cDNA from each sample was used per reaction in a final volume of 20 μl, as described previously [4]. The following primers and probes were purchased from Life Technologies (Applied Biosystems, Carlsbad CA, USA) as TaqMan Gene Expression Assays: NADPH oxidase1 (Nox1), Nox1 organizer (NoxO1), Nox1 activator (NoxA1), $p22^{phox}$, NADPH oxidases 2-3-4-5 (Nox2-3-4-5), Dual oxidases 1 and 2 (Duox1 or 2), and accessory proteins in the cytoplasm: $p22^{phox}$, $p47^{phox}$, $p67^{phox}$, $p40^{phox}$, Rac1, and Rac2. PCR amplification was performed on a 384-well plate using the default cycling conditions (Life Technologies [Applied Biosystems], Carlsbad, CA). Calibration curves for the 18S ribosomal RNA control gene were created using serial dilutions of the plasmid (10^7–1 copy range) containing the gene insert. Relative gene expression was determined as the ratio of the gene of interest to the internal reference gene expression based on the standard curves. The data represent mean values from a minimum of three experiments.

2.3. Assessment of DPI and DTI on reactive oxygen production

The effect of DPI and DTI on tumor cell reactive oxygen production were examined at the whole cell level by measurement of intracellular ROS production by flow cytometry using the redox-sensitive dye CM-H_2-DCF-DA as previously described [5]. In brief, trypsinized cells were counted and 1–2 million cells were treated with 20 nM DPI or 10 μM DTI with continuous shaking at 37 °C for one hr. After centrifugation at 500 × *g* for 2 min, the cell pellets were resuspended in 500 μl HBSS buffer containing the redox sensitive dye at a concentration of 5 μM; the cells were incubated at 37 °C for an additional 30 min. ROS were measured with a Calibur Flow Cytometer (BD BioSciences, Franklin lakes, NJ), and analyzed with FlowJo software (Tree Star Inc., Ashland, OR). The effect of the iodonium analogs on mitochondrial ROS was examined by analytical cytometry using the red fluorescent dye MitoSOX™ [24]. In these experiments, HT-29 cells were exposed to 20 nM DPI or 10 μM DTI for 1 h, centrifuged as described above, and resuspended in HBBS containing 5 μM MitoSOX™ dye for an additional 20 min incubation at 37 °C. Mitochondrial ROS were measured and analyzed by analytical cytometry as specified by the manufacturer. For comparison, we also measured the effect of DPI (20 nM) on both whole cell and mitochondrial ROS levels in HCT-116 human colon carcinoma cells using identical methods.

2.4. Western analysis

HT-29 and HCT-116 cells were harvested during logarithmic phase growth and washed once with PBS; they were then passaged under standard conditions as described above. Cells were exposed to DPI or DTI in complete medium with serum for 48 h; DPI or DTI was removed by washing the cells with PBS. Cytokines were added at a final concentration of 10 ng/ml for 15 min in serum free medium. Cells were washed again in ice cold PBS followed by lysis on the plate in 1× RIPA lysis buffer (Millipore, Temecula, CA, USA) that contained 50 mM Tris (pH 7.4), 150 mM NaCl, 1 mM EDTA, 0.25% deoxycholic acid, 1% NP-40, adding 1–1 tablet/10 ml protease (Complete, mini) and phosphatase (PhosStop) inhibitor cocktails from Roche (Mannheim, Germany). Lysates were left on ice before centrifugation at 10,000 × *g* for 30 min. After protein quantitation using the BCA™ protein assay (Thermo Scientific, Rockford, IL), equal amounts (40–50 μg) of proteins were separated by SDS-PAGE and blotted onto nitrocellulose membranes using the iBlot™ Dry Blotting System from Invitrogen (Invitrogen, Carlsbad, CA). The membrane was blocked with 5% non-fat dry milk in TBST (TBS, pH 7.5, containing 0.1% Tween 20) and incubated with a primary antibody overnight at 4 °C. The following primary antibodies were used: *p*-Erk1/2(Thr202/Tyr204), Erk1/2, *p*-Akt (Ser473), Akt, and *p*-Stat3 (Tyr705) from Cell Signaling Technology Inc. (Danvers, MA, USA); *p*-Stat1 (Tyr701), Stat1, Stat3, *p*-Stat6 (Tyr641), and Stat6 from BD Biosciences (San Jose, CA, USA). The membranes were then washed with TBST and incubated with an appropriate (rabbit or mouse) peroxidase-conjugated secondary antibody (1:5–10,000 dilution) (Santa Cruz Biotechnology, Inc., Santa Cruz, CA, USA) for 1 h at room temperature. Specific antibody binding was detected using the ECL$^+$ detection system (Amersham Biosciences, Little Chalfont Buckinghamshire, UK), according to the manufacturer's recommendations. After development, the membranes were stripped and re-probed with antibody against β-actin (Sigma, St. Louis, MO, USA) to confirm equal sample loading.

2.5. Effect of DPI on protein phosphatase activity

Evaluation of the effect of DPI on protein tyrosine phosphatase (PTP) levels in HT-29 and HCT-116 cells and a normal colonic epithelial cell line was determined using PTP Assay Kit 1 (cat # 17-125, Millipore, Temecula, CA). Following treatment for 48 h with 20 nM DPI that was identical to that performed for Western analysis, cells were scraped in lysis buffer containing 20 mM imidazole–HCl, 2 mM EDTA, 2 mM EGTA pH 7.0 with a protease inhibitor cocktail (Pierce, Rockford, IL cat# 78425), sonicated, and centrifuged at 2000 × *g* for 5 min. The supernatant protein concentration was measured with the BCA protein Assay kit (Pierce, Rockford, IL cat# 23227); 100 ng (normal colonic epithelium) or 500 ng (tumor cells) protein was used per assay well. PTP activity was determined according to the manufacturer's instructions. Briefly, in 96-well (half-volume) plates, we added from 250 ng to 750 ng protein, and 200 μM peptide (RRLIEDAE-pYAARG) in a 25 μl total volume. After incubation for 15 min, the enzyme reaction was terminated with 100 μl Malachite Green solution; a subsequent 15 min was allowed for color development, and absorbance was measured at 650 nm with a plate reader (SpectraMax M5; Molecular Devices, Sunnyvale, CA). Enzyme activity was calculated from the amount of released phosphate in pmol phosphate/min/μg based on a phosphate standard curve.

The effect of DPI on serine/threonine phosphatase levels was examined using the Ser/Thr Phosphatase Assay Kit 1 (cat# 17-127, Millipore, Temecula, CA). Samples were prepared in imidazole buffer, as outlined for the PTP assay; 200 μM peptide (KRpTIRR) substrate, and from 250 ng to 750 ng protein were used per well to determine enzyme activity after a 15 min reaction. The reaction was terminated by the addition of 100 μl Malachite Green solution; and enzyme levels were calculated as described for PTPs.

2.6. Pathway and statistical analyses

Gene lists obtained from the COMPARE algorithm were analyzed with the Ingenuity Pathway Analysis software® (Ingenuity Systems, Redwood City, CA). *P* values for the enrichment of canonical pathways were generated based on the hypergeometric distribution and calculated with the right-tailed Fisher's exact *t*-test for 2 × 2 contingency tables. One-way analysis of variance (ANOVA) post hoc comparisons and intensity plots were calculated and generated using Partek Pro® software 5.1 as previously described [25]. *P* values less than 0.05 were considered significant. All experiments were performed, at minimum, in triplicate.

3. Results

3.1. DPI and DTI demonstrate differential growth inhibitory and cytostatic profiles in the NCI-60 tumor cell line panel

Because the growth inhibitory effects of the iodonium analog DPI have been examined in a limited number of tumor cell models [18,26,27], and that of DTI have not previously been evaluated, we generated growth inhibition and cytotoxicity profiles for DPI and DTI in the NCI-60 panel of human tumor cell lines [20]. An intensity plot of the cell growth inhibitory and cytotoxic actions of DPI and DTI is shown in Fig. 2A. Distinct patterns of growth inhibition were demonstrated across the NCI-60 by these two agents. DPI was substantially more potent than DTI with respect to limiting tumor cell growth, producing a high degree of growth inhibition at concentrations within the low nanomolar range. GI_{50} assays showed that DPI specifically decreased proliferation in four leukemia (CCRF-CEM, K-562, RPMI-8226, and SR), one non-small cell lung cancer (NSCLC) (NCI-H460), one melanoma (SK-MEL-5), and one renal cell line (CAKI-1) at concentrations of ~10 nM (Table 1). Across the entire NCI-60 panel, however, the growth inhibitory effects of DPI varied substantially (Supplementary Fig. 1A); two NSCLC (HOP-62 and NCI-H226), one colon (KM-12), two renal (SN12C and TK-10) and two breast (HS-578T and MDA-MB-231) cancer cell lines demonstrated inhibition of cell proliferation only at concentrations of 3–15 μM (Table 1). In contrast, 1–5 μM DTI was required to achieve the GI_{50} level for the most sensitive members of the panel (Table 1 and Supplementary Fig. 1B). Overall, the GI_{50} for DPI was significantly lower than for DTI across the NCI-60 (Fig. 2B; $P < 0.001$). With respect to the cytostatic (TGI) effects of DPI and DTI on various NCI-60 cell types, DPI produced a cytostatic effect on most cell lines at ~15 μM ($n = 60$); to generate the same cytostatic effect for DTI required a significantly higher mean concentration, ~22 μM ($n = 60$; $P < 0.001$) (Fig. 2B). LC_{50} values, a reflection of cell death that occurs during the 48-h assay, were in the 30–100 μM range for both DPI and DTI (Table 1; Supplementary Fig. 1A and B). We also compared the effect of DPI on the growth of malignant versus non-malignant colonic epithelial cells; the IC_{50} of DPI for the CCD841 line of embryonic colonic epithelium ranged from 75 to 80 nM in multiple experiments where growth inhibition was examined 48 h after drug treatment to simulate conditions used for the NCI-60 panel. This was approximately four-fold higher than that observed for HT-29 cells (20 nM).

3.2. DPI and DTI produce unique patterns of growth inhibition and cytostasis in the NCI-60

To explore potential molecular mechanisms of action of DPI and DTI, we selected 3096 compounds with known or inferred targets

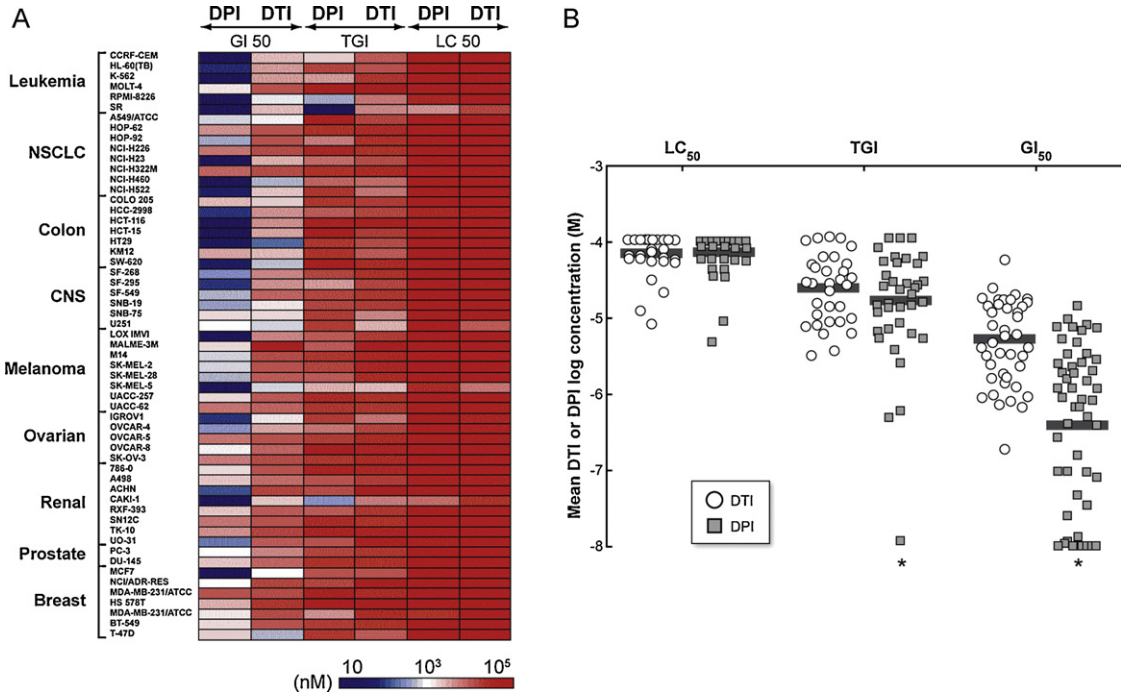

Fig. 2. Effect of DPI or DTI on cell growth across the NCI-60 human tumor cell line panel. (A) Growth inhibition (GI_{50}), cytostatic (TGI), and cytotoxic (LC_{50}) effects of DPI and DTI are demonstrated as an intensity plot created to reveal differential effects of the two compounds on the NCI-60 human tumor cell lines as described in Section 2. The data shown in the figure represent the specific concentrations (nM) of DPI or DTI that produced the GI_{50}, TGI, or LC_{50} for each cell line in the NCI-60 cell panel; the NCI-60 cell lines are grouped by disease subpanels (*Y* axis), and growth inhibition (GI_{50}), cytostatic (TGI) or cytotoxic (LC_{50}) effects (*X* axis). (B) Cytotoxic (LC_{50}), cytostatic (TGI), and growth inhibitory (GI_{50}) actions of DPI and DTI are shown on a logarithmic scale as a scatter plot of the cell lines exposed to either agent in the NCI-60 panel using the same dataset as in (A). The horizontal bars in the figures represent the mean values ($^*P < 0.001$).

as our working dataset from the NCI's public small molecule database, which contains more than 44,000 compounds. The compounds in our working dataset were selected based on the following criteria: (a) at least 2 tests for growth inhibition across the NCI-60 panel had been conducted over a specific concentration range; (b) data were available for at least 50 of the cell lines in the NCI-60; and (c) growth inhibition for at least 5 of the cell lines differed from the mean by at least 0.3 log. Overall evaluation of our results from the COMPARE algorithm demonstrated that the activity patterns of DPI and DTI had no strong correlations [Pearson correlation coefficient (PCC) > 0.7] with the growth inhibitory activities of any of the 3096 compounds in our working database.

As shown in Fig. 3, of the two compounds, DTI demonstrated the more specific activity; however, the cytostatic and cytotoxic associations for DTI were relatively modest, and could be demonstrated for only 4 drugs: diethyldithiocarbamate (a copper chelator and inhibitor of copper–zinc superoxide dismutase [28] (PCC = 0.67), NSC 176324 (PCC = 0.6), amicetin (PCC = 0.51), and azaserine (PCC = 0.53). Moderate associations for DPI with 98 compounds could be grouped into 19 different pharmacological mechanisms, which are shown in Fig. 3. Of specific interest, intermediate growth inhibitory relationships were demonstrable for: topoisomerase II inhibitors (n = 16 drugs, PCC [0.54–0.65]); however, the drugs in this group were all analogs of doxorubicin or daunorubicin that are both known inhibitors of mitochondrial respiration [29]. Mitochondrial poisons, including the electron transport chain inhibitor antimycin A (n = 12, PCC [0.54–0.67]), DNA damaging agents (n = 11, PCC [0.54–0.62]), pseudo nucleotides (n = 9, PCC [0.55–0.68]), alkylating agents (n = 9, PCC [0.54–0.67]), and topoisomerase I inhibitors (n = 8, PCC [0.54–0.59]) were the other large groupings of agents that associated with the pattern of growth inhibition produced by DPI in the NCI-60 panel.

3.3. Expression of NADPH oxidase and accessory genes in the NCI-60 tumor cell panel and the relationship of NADPH oxidase expression to tumor cell growth inhibition by DPI and DTI

Since the discovery of the Nox gene family [30], DPI and DTI have regularly been employed as Nox inhibitors, despite the pleiotropic nature of their molecular actions [13,31]. Because members of the Nox family have been shown to have important effects on cell proliferation [32,33], and because of the known inhibitory activity of DPI and DTI on this family of membrane oxidases, we examined RNA expression of Nox family members (as well as their critical accessory genes) across the NCI-60 to evaluate whether Nox expression and the antiproliferative actions of DPI or DTI were related. Expression levels of Nox genes 1–5, and the NADPH dual oxidases (Duox1 and 2), relative to 18S rRNA, in the NCI-60 human cancer cell line panel are shown in Fig. 4 and Supplementary Table 1. Expression was arbitrarily graded as low (Nox copy number/18S rRNA ratio $<500 \times 10^{-8}$), intermediate (ratio >500 but less than 2000×10^{-8}), or high (ratio $>2000 \times 10^{-8}$). Nox genes with expression ratios $>500 \times 10^{-8}$ were routinely visible by Northern analysis using >40 μg total RNA (data not shown). Low levels of Nox 1, 2, 5, Duox1, and the Nox accessory genes NoxO1, p40, p47, and p67 were detected in half of the cell lines; no detectable to low levels of Nox2 and Duox2, and the accessory genes NoxA1, p22, Rac1 and Rac2 were found in one third of the cell lines. Overall, high levels of Nox gene expression were found in ~15% of the NCI-60 panel.

Intermediate to high levels of Nox1 mRNA expression were observed in HT-29 colorectal and NCI-H226 NSCLC cell lines, respectively. The majority of the cell lines in the NCI-60 panel have very low or virtually undetectable levels of Nox1 expression. Nox2 expression was observed at high levels in two leukemia cell lines (HL-60-TB and RPMI-8226). The other cell lines in the NCI-60 cell line panel did not express Nox2. Nox3 mRNA was not detectable in

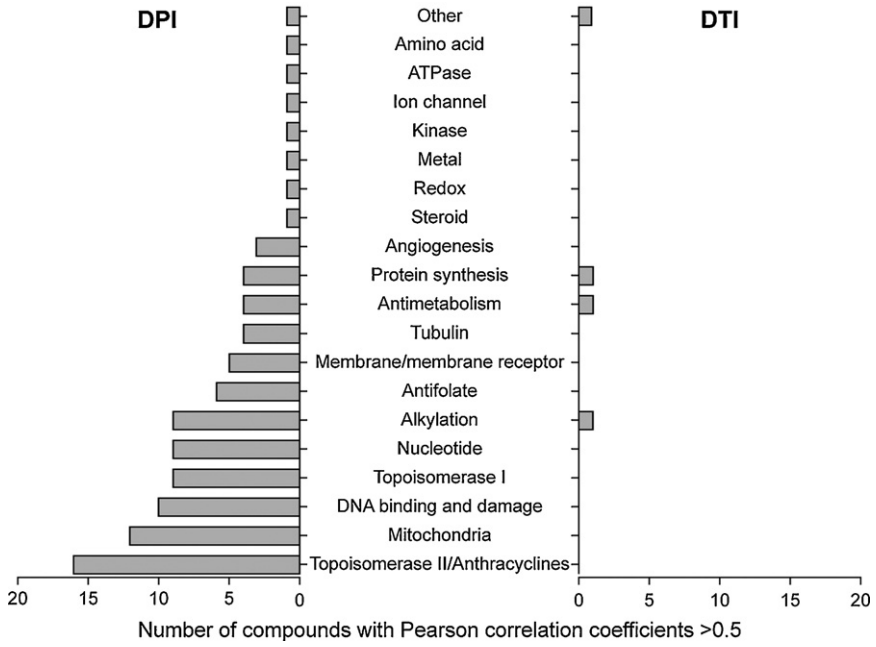

Fig. 3. Anticancer compounds in the NCI small molecule database classified by known mechanisms of action whose growth inhibitory profiles (GI_{50}) correlate across the NCI-60 with those of DPI and DTI (PCC > 0.5).

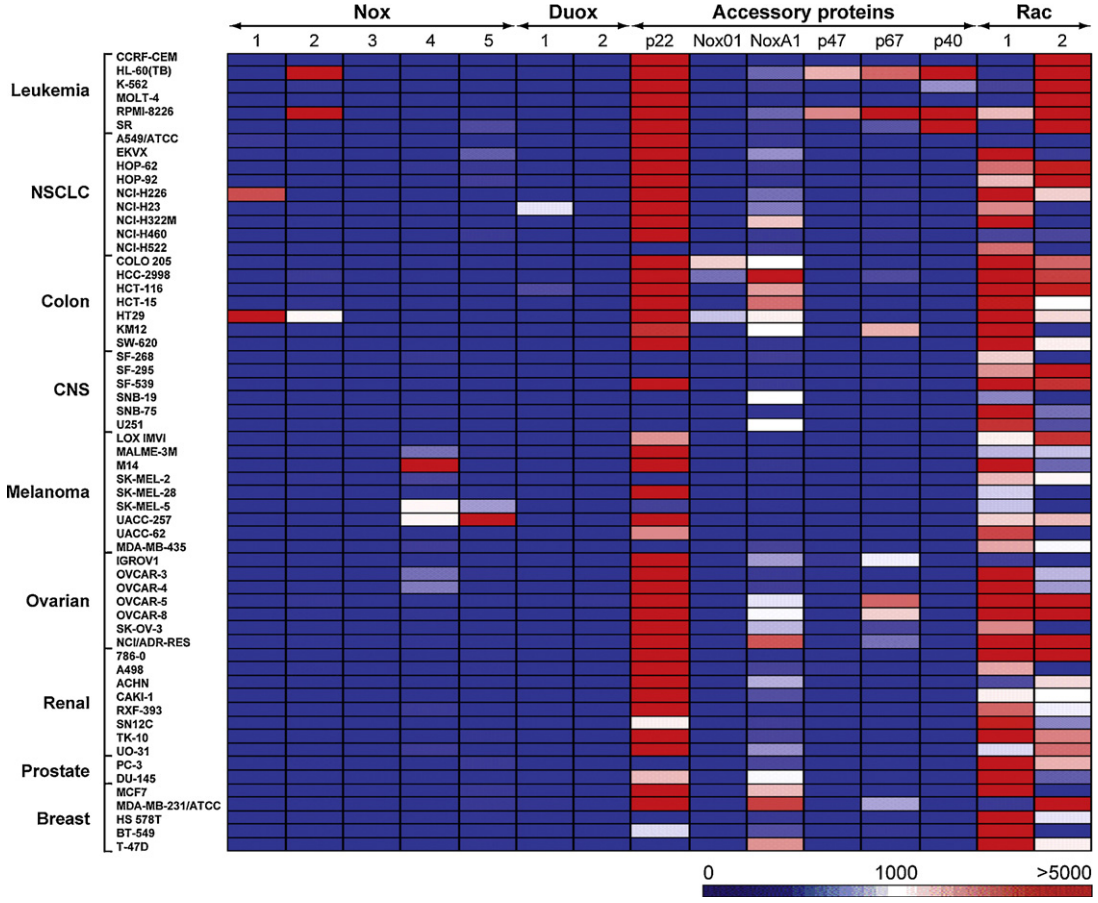

Fig. 4. Intensity plot of mRNA expression of Nox isoforms and accessory genes in the NCI-60 tumor cell panel relative to 18S rRNA levels. The data represent the relative mRNA expression ratios (from undetectable to >5000) for all of the cells in the NCI-60 panel; the expression ratios are grouped by disease subpanels (*Y* axis), and Nox family or accessory gene expression (*X* axis); the data represent the mean values from a minimum of three experiments.

any of the cell lines in the NCI-60 panel. Nox4 expression was virtually undetectable in 80% of the cells. However, high and intermediate Nox4 expression was demonstrable in several melanoma lines (M14, UACC-257, SK-MEL-5, MALME-3M and SK-MEL-2), as well as CCD841 non-malignant colonic epithelial cells (which were essentially devoid of other Nox isoforms; Supplementary Table 1). Ovarian cancer cell lines, such as OVCAR-3 and OVCAR-4, also expressed intermediate levels of Nox4. Nox5 expression was high only in melanoma cell lines. High or intermediate level expression of Duox1 was found in NCI-H23 NSCLC cells and the HCT-116 colon cancer line. Virtually all other cell lines demonstrated undetectable or very low levels of Duox1 or Duox2 expression.

Critical levels of several accessory gene products are required to produce the multicomponent complexes needed for functional Nox1, 2, and 3 as well as Duox1 and 2 oxidase activity [1]. Therefore, our current study included an evaluation of the expression of the accessory genes needed to support oxidase function across the NCI-60. Of the accessory genes tested, high expression levels of $p22^{phox}$ were present in most cell lines (Supplementary Table 1). The exceptions are the NSCLC line NCI-H522, the CNS lines SF-268, SF-295, SNB-19, SNB-75 and U251, melanomas SK-MEL-2 and SK-MEL-5, PC-3 prostate cancer cells, as well as breast cell lines HS578T and T-47D where virtually undetectable levels of $p22^{phox}$ were observed. Intermediate expression levels of NoxO1, the homologue of $p47^{phox}$ in epithelial cells, were found only in three colon cancer cell lines (Colo-205, HCC-2998, and HT-29). mRNA expression of NoxA1, the epithelial homolog of $p67^{phox}$, was found at intermediary to high levels in most colon cancer and some breast cancer and NSCLC lines. Expression levels of other accessory genes including members of the Nox2 complex that were initially described as part of the granulocyte membrane oxidase ($p67^{phox}$, $p47^{phox}$, and $p40^{phox}$) [34] were found predominantly in tumor cells of hematopoietic lineage (HL-60 and RPMI-8226).

Association with the small guanine nucleotide-binding proteins Rac1 and/or Rac2 is normally required for full enzymatic activity of Noxs and Duoxs [1]. Hence, we also measured the expression patterns of Rac1 and 2 across the NCI-60 cancer cell line panel. We found that Rac1 expression is ubiquitous, but varied over a 3–8-fold range in the different cell lines, with low level expression in most leukemia cells and the highest in T-47D breast cancer cells. Rac2 was expressed at significantly higher levels than Rac1 across all leukemia cell lines. Five of the NSCLC cell lines demonstrated minimal expression of Rac2.

We performed pair wise comparisons of the growth inhibitory effects of DPI and DTI against the expression levels of the members of the Nox gene family across the NCI-60 panel. Nox1 expression was found to be modestly correlated with the TGI and the LC_{50} values for DPI in the panel, with a PCC of 0.49 for each. No correlation between Nox expression and tumor growth inhibition by DTI was observed for the NCI-60 panel.

3.4. Relationships between the pattern of Nox gene expression and specific molecular pathways evaluated by expression array profiling of the NCI-60

We also examined potential relationships between the expression profile of the Nox family across the NCI-60 and functional pathways known to be present in these cells. The major biological functions that correlated significantly with Nox1 expression levels are shown in Supplementary Table 2; these included genes associated with cytokine signaling (IL-6, Jak/Stat), the mitogen-activated protein (MAP) kinase pathway, and cell cycle progression. For the entire Nox gene family, Ingenuity pathway analysis (IPA) revealed strong correlations between Nox expression and inflammatory and immune response pathways, the G_1 to S transition, and cell growth and proliferation (Table 2).

Table 2
Relationship of Nox family gene expression to baseline mRNA expression of specific molecular pathways in the NCI-60 cell panel.

	P value	No. of molecules
Disease and disorders		
Connective tissue disorders	<0.03	28
Inflammatory disease	<0.03	31
Skeletal and muscular disorders	<0.03	28
Genetic disorder	<0.03	61
Immunologic disease	<0.04	33
Molecular and cellular functions		
Cellular growth and proliferation	<0.03	37
Cell-to-cell signaling and interaction	<0.04	44
Cell cycle	<0.03	10
Physiological system development and function		
Hematological systems development and function	<0.03	35
Humoral immune response	<0.03	29
Tissue morphology	<0.03	21
G1/S transition of the cell cycle	<0.04	11
Hematopoiesis	<0.03	19

3.5. Predicting molecular targets of DPI and DTI from the correlation of their NCI-60 growth inhibition patterns and baseline gene expression profiling of the tumor cell panel by mRNA expression microarrays

To explore additional molecular mechanisms of action of DPI and DTI in the NCI-60 panel using the COMPARE algorithm, we evaluated correlations between the pattern of growth inhibition produced by these drugs and a "consensus" dataset of mRNA expression levels for the NCI-60. A total of 435 genes were found where the pair wise *P* value was <0.0005, and at least 2 tests for correlation were >0.5 from the correlation of NCI-60 Affymetrix® gene expression profiling and the cytotoxic and cytostatic patterns of DPI and DTI. In addition to the purely statistical correlation analysis, we employed the IPA Knowledge database (www.ingenuity.com) to improve our understanding of the biological consequences of DPI and DTI treatment. The 435 genes were mapped to 45 canonical pathways as defined by the IPA tool with $P < 0.05$. These 45 canonical pathways could be arbitrarily grouped into inflammatory and cytokine-related signaling that primarily involved the Jak/Stat pathway, growth factor and steroid receptor-related signaling, mitochondrial pathways and membrane functions, as well as retinol and neuron related signaling (Fig. 5).

In general, more canonical pathways could be correlated with the response of the NCI-60 tumor cell lines to DPI ($n = 17$) than to DTI ($n = 10$). However, the growth inhibitory effects of both compounds appeared to be related to the expression in the NCI-60 cell lines of components of the Jak/Stat pathway as well as various cytokine signaling cascades, expression of the genes controlling the citric acid cycle, VEGF signaling, and a variety of membrane receptors critical for tumor cell proliferation (estrogen and ephrin receptors, for example).

3.6. Evaluation of the effects of DPI and DTI on reactive oxygen metabolism in HT-29 and HCT-116 cells

To examine potential relationships between the effects of DPI and DTI on the production of ROS, growth inhibition, and signaling pathways that could be involved in the mechanism(s) of action of iodonium analogs, we measured steady state levels of ROS in HT-29 cells following DPI or DTI treatment (Fig. 6). A 1-h exposure to the GI_{50} concentrations of either DPI (Fig. 6A) or DTI (Fig. 6B),

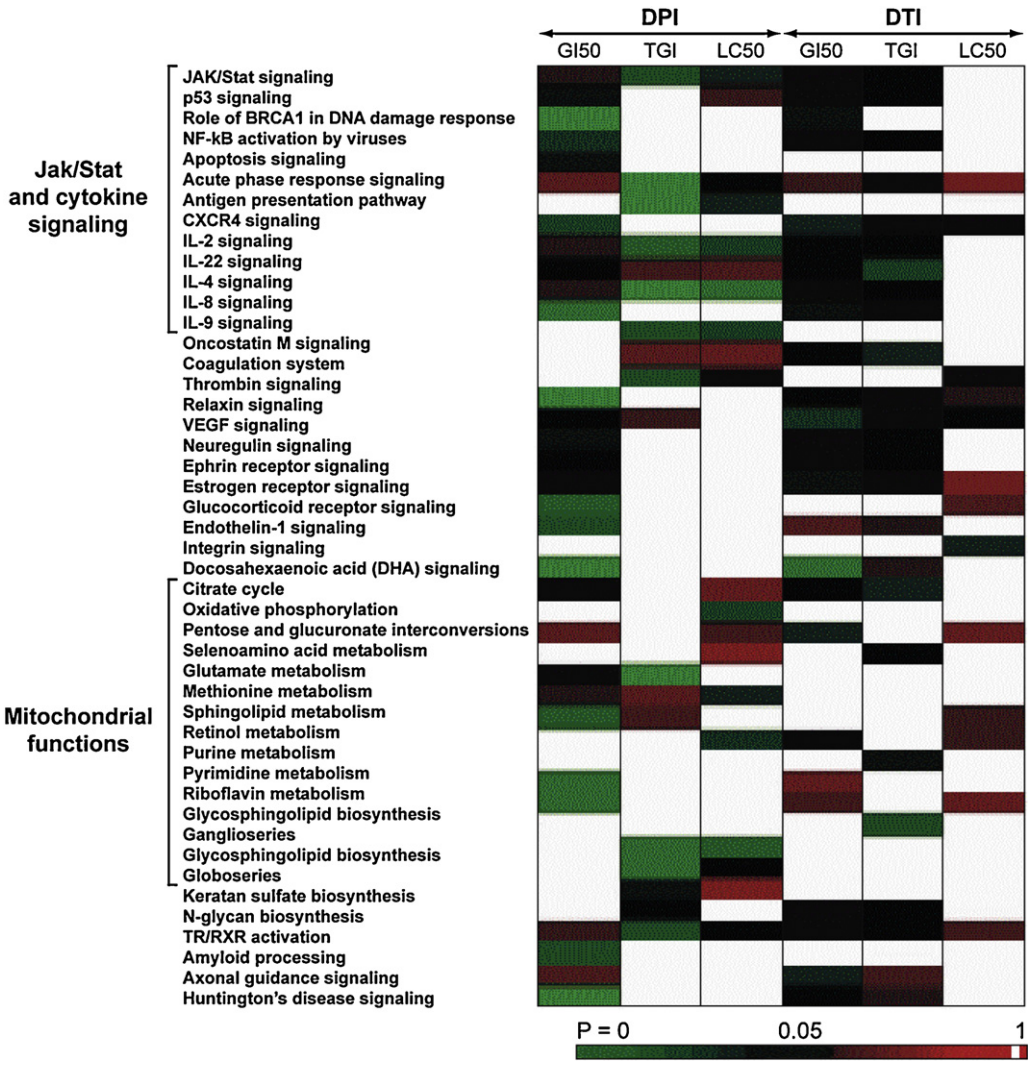

Fig. 5. Prediction of molecular signaling pathways modulated by DPI or DTI based on the cytostatic and cytotoxic patterns of these agents in the NCI-60 cell panel. An intensity plot of *P* values for individual signaling pathways is shown to examine potential differential effects of the test compounds on signal transduction.

decreased whole cell ROS levels. On the other hand, mitochondrial ROS production measured with the redox-active dye MitoSOX™ was not inhibited by DPI under the same experimental conditions (Fig. 6C); and DTI appeared to slightly increase ROS levels after a 1-h exposure to a 10 μM concentration of the agent (Fig. 6D). For comparative purposes, we evaluated the effect of an equimolar concentration of DPI on ROS in HCT-116 cells that lack Nox1. As shown in Fig. 6E, DPI decreases ROS levels in HCT-116 colon cancer cells measured as whole cell DCF fluorescence, albeit to a lesser degree than in the HT-29 line. However, unlike HT-29 cells, DPI (20 nM) also decreased mitochondrial ROS levels in the HCT-116 tumor line (Fig. 6F).

3.7. Qualification of predicted mechanisms of action for DPI and DTI

To evaluate directly the predicted effect of the iodonium analogs on signal transduction through the Jak/Stat and/or MAP kinase pathways, we exposed HT-29 human colon cancer cells (that express Nox1 and are part of the NCI-60 panel) to growth inhibitory concentrations of DPI (20 or 30 nM), DTI (10 or 15 μM), or an equal concentration of DMSO for 48 h. At the completion of DPI, DTI, or DMSO exposure, tumor cells were treated with one of the following cytokines (or a vehicle or iodonium analog control) that are known to affect the proliferative capacity of intestinal epithelial cells: IL-4, IL-6, IL-13, or IL-22 [35–37]. As shown in Fig. 7A, DPI exposure substantially decreased the activation of Stat1 and Stat3 by all four cytokines, and produced a modest decrease in the levels of phosphorylated Stat6 and total Stat6 after exposure to IL-4 or IL-13. The phosphorylation of Erk1/2 and Akt produced by each of the growth-promoting cytokines was also inhibited by DPI (Fig. 7B). On the other hand, DTI decreased IL-6-induced activation of Stat1 and Stat3, and IL-4-related phosphorylation of Stat6, but did not affect Stat phosphorylation produced by the other cytokines (Fig. 7C). However, like DPI, DTI also substantially decreased Erk1/2 and Akt phosphorylation that had been enhanced by IL-4, IL-13, IL-6, or IL-22 (Fig. 7D). We also examined, under identical conditions, the effects of DPI (20 nM) and DTI (10 μM) on IL-4- and IL-6-mediated phosphorylation of Erk1/2 and Akt in HCT-116 cells that do not express Nox1 (Supplemental Table 1). The effect of the iodonium analogs on signal transduction through the Jak/Stat pathway could not be evaluated with HCT-116 cells because of the irregular nature of Stat activation by the cytokines in this cell line. However, we did find that neither DPI (Fig. 7E) nor DTI (Fig. 7F) altered IL-4- or IL-6-mediated Erk1/2 or Akt phosphorylation or protein expression in HCT-116 cells.

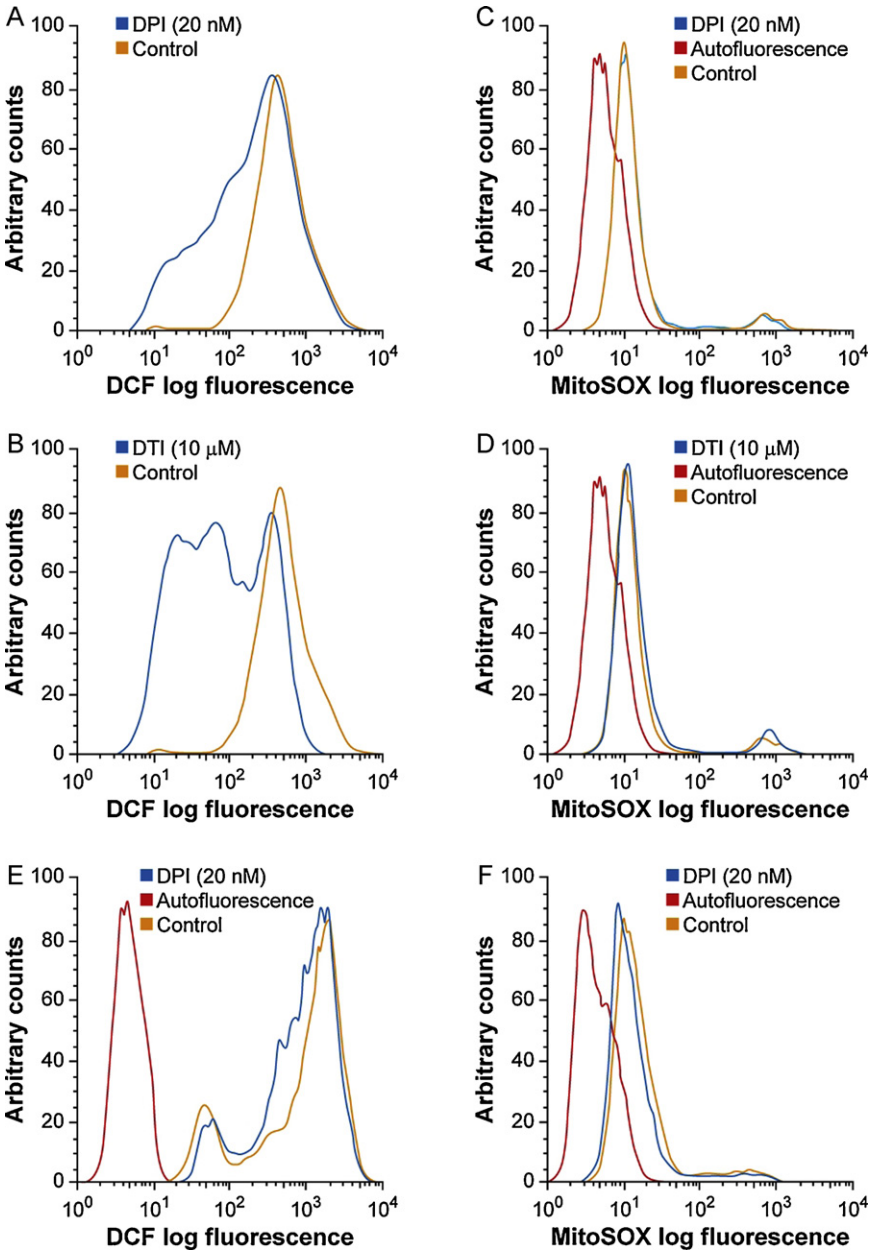

Fig. 6. Evaluation of the effects of DPI and/or DTI on whole cell and mitochondrial reactive oxygen production in HT-29 and HCT-116 human colon cancer cells. In panels (A) and (B), the effects of a 1-h exposure of HT-29 cells to either DPI (20 nM) or DTI (10 μM) on steady state levels of ROS were measured by the fluorescence of the dye DCFH-DA following conversion to DCF. Panels (C) and (D) demonstrate the intrinsic autofluorescence of HT-29 cells, the steady state levels of mitochondrial ROS (control) as represented by the fluorescence of the redox active mitochondrial dye MitoSOX™, and the effects of DPI and DTI on mitochondrial ROS. In panel (E), the effect of a 1-h exposure of DPI (20 nM) on steady state levels of ROS in whole HCT-116 cells was examined by the conversion of DCFH-DA to DCF. Panel (F) demonstrates the effect of DPI on mitochondrial ROS levels in HCT-116 cells measured with the MitoSOX™ reagent. The data shown are representative of multiple experiments with each compound and both redox-active dyes.

Because IL-4-mediated enhancement of reactive oxygen production in keratinocytes, with a consequent inhibition of protein phosphatase activity, has recently been proposed as an explanation for increased Stat6 phosphorylation in those cells [38], we evaluated the effect of DPI on both protein tyrosine and serine/threonine phosphatase activities in HT-29 and HT-116 colon cancer cells, and in CCD841 normal colonic epithelial cells (Table 3). We found that DPI (20 nM) exposure for 48 h led to a significant increase in both tyrosine and serine/threonine phosphatase activities in HT-29 cells but had no effect on those phosphatases in the HCT-116 line. Furthermore, DPI significantly inhibited phosphatase levels in normal colonic epithelial cells (Table 3).

4. Discussion

In this study, we examined the antiproliferative effects of the flavoenzyme inhibitors DPI and DTI in the NCI-60 panel of human tumor cells. Previous studies of the anticancer activity of these agents have been limited to a small number of human tumor cell lines exposed only to DPI, most often at concentrations $\geq$2.5 μM [18,19,26]. Our goals in this investigation were to compare the pharmacologic behaviors of DPI and DTI, and to predict possible molecular targets and mechanisms of action of DPI and DTI using the COMPARE program to evaluate activity profiles of these agents against the expression profile of Nox genes and the baseline expression patterns of canonical gene pathways in the NCI-60.

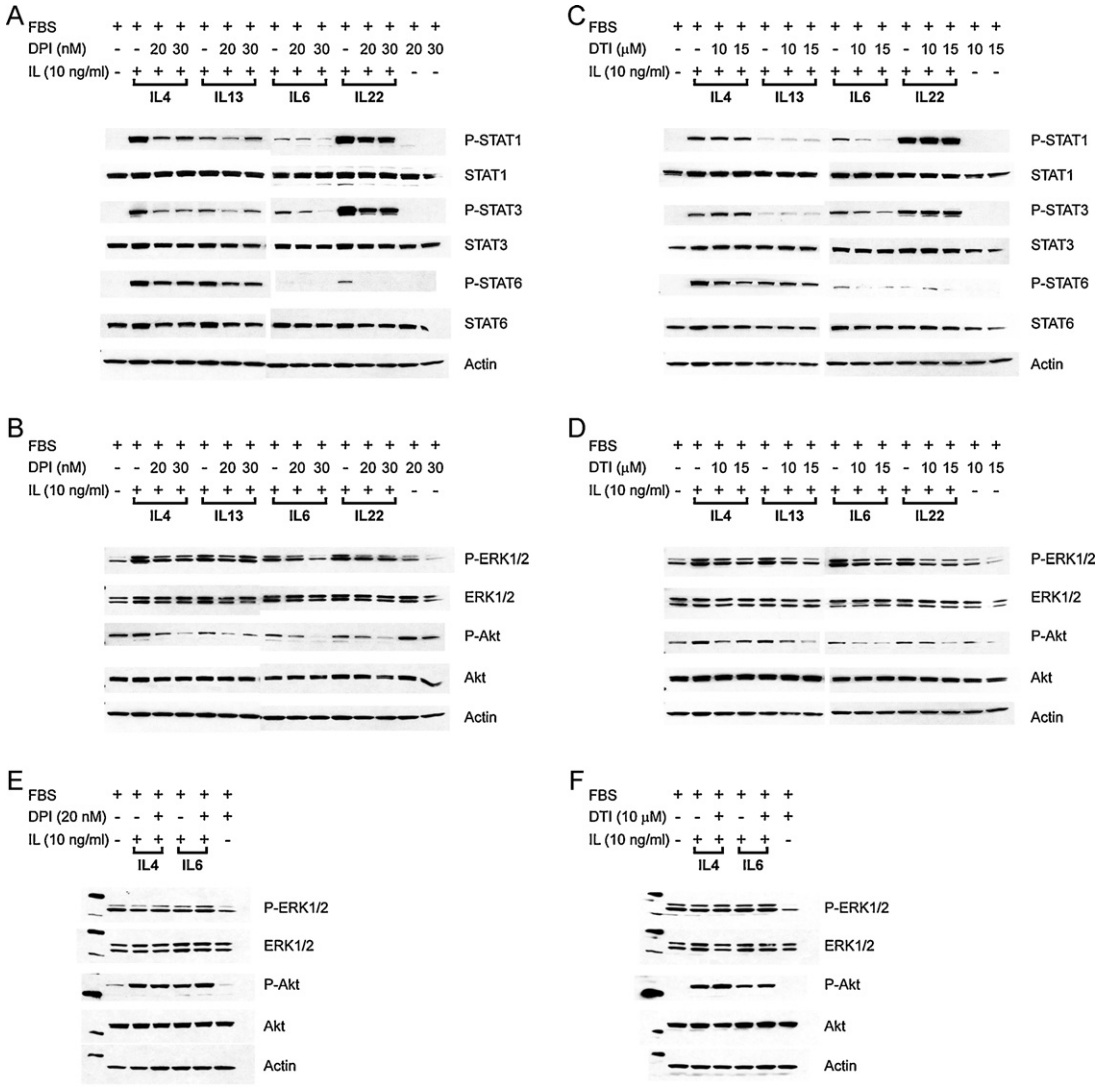

Fig. 7. Effect of exposure of HT-29 and HCT-116 human colon cancer cells to DPI or DTI on cytokine-induced signal transduction through the Jak/Stat, Erk, and Akt pathways. (A) and (B) represent the effects of DPI exposure (20 or 30 nM) for 48 h on the subsequent activation of the Jak/Stat, Erk, and Akt pathways in HT-29 cells following treatment with IL-4, IL-13, IL-6, or IL-22. (C) and (D) demonstrate the effects of DTI exposure at concentrations of 10 or 15 μM for 48 h on Jak/Stat, Erk, and Akt activation in HT-29 cells treated with IL-4, IL-13, IL-6, or IL-22. (E) and (F) represent the effects of DPI (20 nM) and DTI (10 μM), respectively, on IL-4 and IL-6 activation of Erk and Akt signaling in HCT-116 human colon cancer cells. Cytokine exposure was for 15 min at a concentration of 10 ng/ml. DPI and DTI concentrations were chosen because they represent approximations of the GI_{50} values for both compounds in the NCI-60 panel.

We found that DPI inhibited tumor cell proliferation more potently than DTI, with a GI_{50} of ~10 nM versus ~1–4 μM for DTI in human leukemia cell lines (Table 1). For the entire NCI-60 panel, DPI was significantly more active than DTI with respect to GI_{50} and TGI, $P < 0.001$ (Fig. 2A and B). Much higher concentrations of either agent (>10–20 μM) were required for cytotoxicity in any of the cell lines examined. These results suggest that the antiproliferative effects of iodonium analogs occur at substantially lower drug levels in human tumor cell lines than previously suggested, <250 nM for DPI [19]. Furthermore, since many prior investigations of the biochemical effects of DPI were performed utilizing much higher drug concentrations (>2.5 μM) [18,26], our data are consistent with the possibility that the range of antiproliferative mechanisms of action of DPI may be broader than previously surmised.

When the pattern of growth inhibition in the NCI-60 produced by the iodonium analogs was evaluated against ~3000 anticancer agents with known mechanisms of action utilizing the COMPARE algorithm, the activity of DTI was found to be highly distinct; only the copper/zinc chelating agent and superoxide dismutase inhibitor diethyldithiocarbamate, which can produce both oxidant

Table 3
Effect of a 48-h DPI exposure on protein phosphatase levels in colon cancer and normal colonic epithelial cells.

Cell line	Tyrosine phosphatase control	Tyrosine phosphatase DPI (20 nM)	Ser/Thr phosphatase control	Ser/Thr phosphatase DPI (20 nM)
HT-29	56.9 ± 2.5[a]	100.7 ± 10.1*	95.1 ± 5.1	127.6 ± 6.7*
HCT-116	139.3 ± 4.8	121.6 ± 14.1	167 ± 18.4	144.6 ± 7.7
CCD841	362.9 ± 11.3	192.3 ± 9.1*	354.7 ± 18.7	203.6 ± 10.5*

[a] Phosphatase activity expressed as pmol phosphate/min/μg protein ± SD.
* $P < 0.01$.

and non-oxidant effects in vivo [39,40], had a PCC > 0.65 when compared to DTI. Although no strong mechanistic associations (PCC > 0.70) were demonstrable for DPI, intermediate growth inhibitory relationships were found for 98 compounds; 28 of the 98 were either direct mitochondrial poisons or anthracycline antibiotics known to interfere with mitochondrial metabolism [41]. The effects of DPI on mitochondrial electron transport are well established [8,16], and may contribute to DPI-induced mitochondrial reactive oxygen production and apoptosis in the HL-60 human promyelocytic tumor cell line [26]. The growth inhibitory pattern exhibited by DPI also demonstrated some degree of similarity to drugs that affect the mitotic apparatus and those that have anti-angiogenic properties. These observations are of interest because of studies that have shown experimentally that DPI inhibits cell cycle progression by blocking entry into mitosis [17], and at much lower drug concentrations, by inducing a p21-dependent block at G_1 [42]. Furthermore, DPI also induces apoptosis in human vascular endothelial cells [43], perhaps helping to explain its anti-angiogenic activity.

Because of the extensive use of DPI as an inhibitor of Nox function, and the role of the Nox family in cell proliferation [44], we examined the relationship between the patterns of growth inhibition produced by DPI and DTI and the expression of Nox family genes in the NCI-60 tumor cell panel. We found that growth inhibition by DPI, but not DTI, correlated moderately with the level of Nox1 in the cell lines of the NCI-60. One explanation for this observation is the relatively modest degree of expression of Nox1 in this panel, where only the HT-29 colon cancer and NCI-H226 NSCLC lines demonstrated intermediate to high levels of Nox1 mRNA. Although a limited comparison, we also found that the normal colonic epithelial cell line CCD841, which lacks Nox1 but does express Nox4, demonstrated a four-fold higher IC_{50} for DPI than HT-29 cells. This observation may assist further studies of the selectivity of agents that inhibit Nox activity. On the other hand, a comparison of the overall pattern of Nox gene expression in the NCI-60 with the expression of specific gene families in canonical pathways of the same cells, determined using the Ingenuity® analysis program, revealed (Table 2) that inflammatory and immune functions, as well as cell growth and cell cycle transition (G_1 to S), correlated significantly with Nox expression. These results are of interest because of recent studies demonstrating that Nox1, Nox4, Nox5, and Duox2 all play an important role in mediating critical signal transduction pathways initiated by the immuno-modulatory and pro-inflammatory cytokines interleukin-4 (IL-4), interleukin-13 (IL-13), and interferon-γ [5,35,45].

A role for altered cytokine signaling in the mechanism of action of DPI and DTI (that could occur, at least in part, by inhibition of Nox- or mitochondrion-related ROS formation) was also suggested by our evaluation of the biological functions of the genes and canonical pathways in the NCI-60 that were found to correlate significantly with the inhibitory profiles produced by DPI and DTI in these cells (Fig. 5). Signal transduction via the Jak/Stat pathway for interleukins 2, 4, 8, and 22 were all predicted to correlate with inhibition of cell growth produced by the iodonium analogs. These observations are not surprising, since it has been known for some time that the activation of Stat1 and Stat3 can be enhanced by

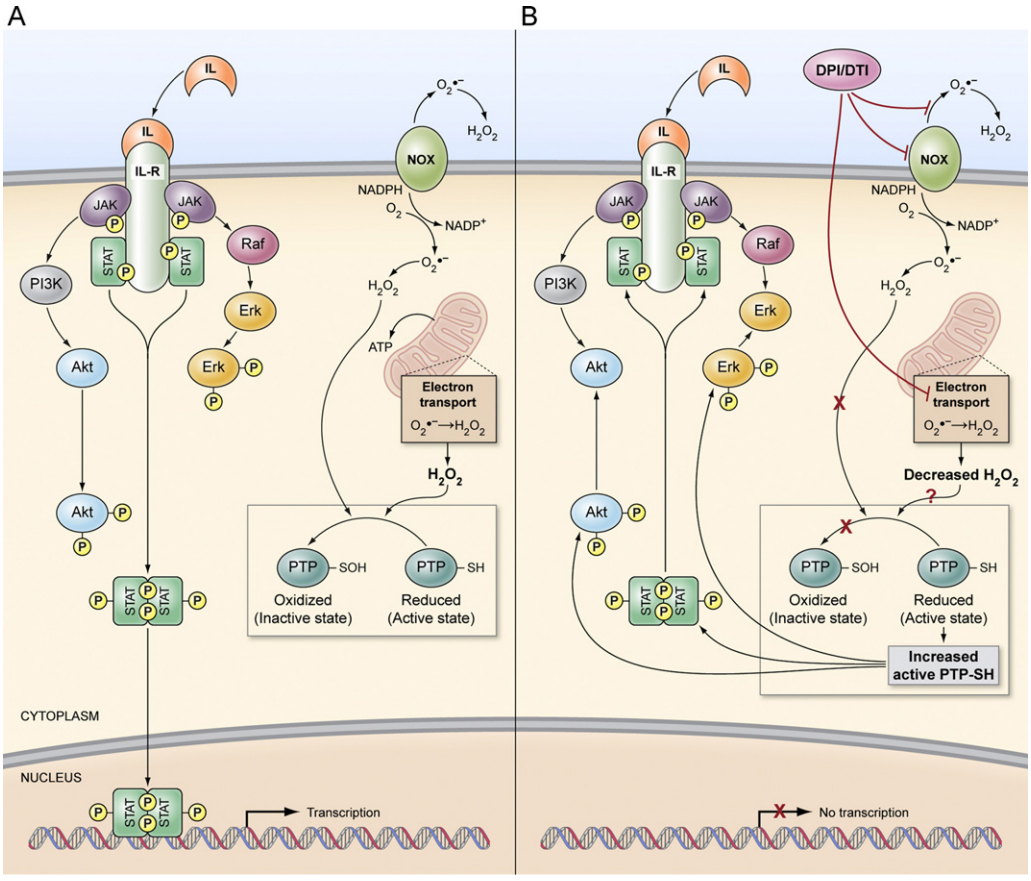

Fig. 8. Model for the potential role of altered cytokine-mediated signal transduction and mitochondrial metabolism in DPI- and DTI-related growth control. In this hypothetical model, activation of the Jak/Stat pathway (A) is blocked by drug-induced inhibition of ROS production from Nox isoforms that results in an enhancement of intracellular phosphatase activity (B). Whether DPI- or DTI-related alterations in mitochondrial ROS affect intracellular phosphatases remains speculative, and is probably cell context dependent, as indicated by the question mark in the figure. DPI or DTI may also directly or indirectly modify cell proliferation downstream of Jak/Stat by way of the Ras or PI3K pathways through dephosphorylation of Erk1/2 and/or Akt, or by direct effects on oxidative phosphorylation and other mitochondrial metabolic pathways distinct from the generation of ROS.

hydrogen peroxide or growth factor-induced ROS [46,47], as well as by exposure to the cytokine interleukin-22 [36]. Furthermore, signaling through IL-4 or 13 in keratinocytes appears to upregulate Duox1, increasing H_2O_2 production and subsequent oxidative inactivation of the phosphotyrosine phosphatase PTP1B; decreased phosphatase activity following cytokine exposure is then responsible for enhancing Stat6 phosphorylation [38]. By analogy, interruption of Jak/Stat-mediated signaling pathways by DPI and DTI, possibly related to a drug-induced decrease in ROS, and subsequent enhancement of phosphatase function, provides a plausible explanation for at least part of the antiproliferative activity of these compounds.

To evaluate these possibilities experimentally, we measured both whole cell and mitochondrial ROS after exposure of HT-29 cells to DPI or DTI (Fig. 6). We found that both iodonium analogs decreased ROS production in intact cells but not in mitochondria at concentrations that were associated with an inhibition of Jak/Stat, Erk1/2, and Akt activation and a significant increase in phosphatase activity in HT-29 cells (Fig. 7 and Table 3). To develop a better understanding of the importance of Nox1 as a target of DPI (versus the electron transport chain), we also examined the effect of the agent on ROS levels in HCT-116 cells that lack Nox1. As shown in Figs. 6E and F, while DPI exposure decreased DCF fluorescence in the HCT-116 line (a measure of whole cell ROS), albeit to a lesser degree than in HT-29 cells, mitochondrial ROS levels were also diminished. It is possible that the observed decrease in mitochondrial ROS may have contributed to the results observed with DCF, and may help to explain the lack of a significant change in phosphatase activity (that is often extramitochondrial) in HCT-116 cells.

Inhibition of components of the MAPK pathway, downstream of Stat activation, are likely to have contributed to the antiproliferative effect of DPI and DTI [48], and could help to explain the DPI-related G_1 block in the cell cycle that has been reported previously [42]. Inhibition of Akt phosphorylation by these agents was also observed and may be related to decreased proliferation in HT-29 cells [49]. On the other hand, DPI neither altered Erk1/2 or Akt signaling or phosphatase activity in HCT-116 cells that lack Nox1.

Furthermore, as shown in Fig. 3, a moderate association was demonstrated by the COMPARE program between the pattern of growth inhibition produced by DPI in the NCI-60 panel and that observed for the anthracycline antibiotics. In a recent study, doxorubicin was found to significantly inhibit Erk1/2, Akt, and Stat3 phosphorylation in rat neonatal cardiomyocytes [50]. Thus, it is not unreasonable to suggest some similarity between the mechanisms of growth inhibition produced by DPI and the anthracycline antibiotics.

In conclusion, as modeled in Fig. 8, our studies suggest that DPI and DTI are members of a unique class of compounds that have profound effects not only on the flavoproteins needed to maintain intracellular oxidative tone, such as Nox proteins or members of the electron transport chain [51], and on the reducing equivalents required for redox homeostasis (pentose phosphate shunt), but also, at nanomolar concentrations, on essential redox-sensitive cytokine signaling pathways that are necessary for tumor cell growth, angiogenesis, and immune function. Although our data support the model proposed in Fig. 8, it must be recognized that the antiproliferative effects of these agents are almost certainly pleiotropic; understanding the most critical of such effects in tumor cells will require further experimental evaluation utilizing drug concentrations that are relevant to alterations in growth. Hence, the effects of low concentrations of the iodonium analogs on cytokine-related signal transduction demonstrated in our current studies are likely to be only an initial reflection of the variety of molecular pathways that are involved in the novel profile of growth inhibition produced by these agents in the NCI-60 human tumor cell line panel.

Conflicts of interest

None declared.

Acknowledgments

This work was supported in whole or in part with federal funds from the Center for Cancer Research and the Division of Cancer Treatment and Diagnosis, National Cancer Institute, National Institutes of Health. The content of this publication does not necessarily reflect the views or policies of the Department of Health and Human Services, nor does mention of trade names, commercial products, or organizations imply endorsement by the US Government.

Appendix A. Supplementary data

Supplementary data associated with this article can be found, in the online version, at doi:10.1016/j.bcp.2012.01.022.

References

[1] Bedard K, Krause KH. The NOX family of ROS-generating NADPH oxidases: physiology and pathophysiology. Physiol Rev 2007;87:245–313.
[2] Kamata T. Roles of Nox1 and other Nox isoforms in cancer development. Cancer Sci 2009;100:1382–8.
[3] Brown DI, Griendling KK. Nox proteins in signal transduction. Free Radic Biol Med 2009;47:1239–53.
[4] Juhasz A, Ge Y, Markel S, Chiu A, Matsumoto L, van Balgooy J, et al. Expression of NADPH oxidase homologues and accessory genes in human cancer cell lines, tumours and adjacent normal tissues. Free Radic Res 2009;43:523–32.
[5] Wu Y, Antony S, Juhasz A, Lu J, Ge Y, Jiang G, et al. Up-regulation and sustained activation of Stat1 are essential for interferon-gamma (IFN-gamma)-induced dual oxidase 2 (Duox2) and dual oxidase A2 (DuoxA2) expression in human pancreatic cancer cell lines. J Biol Chem 2011;286:12245–56.
[6] Pelicano H, Carney D, Huang P. ROS stress in cancer cells and therapeutic implications. Drug Resist Update 2004;7:97–110.
[7] Xia C, Meng Q, Lin LZ, Rojanasakul Y, Wang XR, Jiang BH. Reactive oxygen species regulate angiogenesis and tumor growth through vascular endothelial growth factor. Cancer Res 2007;67:10823–30.
[8] Holland PC, Clark MG, Bloxham DP, Lardy HA. Mechanism of action of the hypoglycemic agent diphenyleneiodonium. J Biol Chem 1973;248:6050–6.
[9] Gatley SJ, Sherratt HS. The effects of diphenyleneiodonium and of 2,4-dichlorodiphenyleneiodonium on mitochondrial reactions. Mechanism of the inhibition of oxygen uptake as a consequence of the catalysis of the chloride/hydroxyl-ion exchange. Biochem J 1976;158:317–26.
[10] Stuehr DJ, Fasehun OA, Kwon NS, Gross SS, Gonzalez JA, Levi R, et al. Inhibition of macrophage and endothelial cell nitric oxide synthase by diphenyleneiodonium and its analogs. FASEB J 1991;5:98–103.
[11] Cross AR, Jones OT. The effect of the inhibitor diphenylene iodonium on the superoxide-generating system of neutrophils. Specific labelling of a component polypeptide of the oxidase. Biochem J 1986;237:111–6.
[12] O'Donnell BV, Tew DG, Jones OT, England PJ. Studies on the inhibitory mechanism of iodonium compounds with special reference to neutrophil NADPH oxidase. Biochem J 1993;290(Pt 1):41–9.
[13] Aldieri E, Riganti C, Polimeni M, Gazzano E, Lussiana C, Campia I, et al. Classical inhibitors of NOX NAD(P) H oxidases are not specific. Curr Drug Metab 2008;9:686–96.
[14] Pazhanisamy SK, Li H, Wang Y, Batinic-Haberle I, Zhou D. NADPH oxidase inhibition attenuates total body irradiation-induced haematopoietic genomic instability. Mutagenesis 2011;26:431–5.
[15] Honore S, Kovacic H, Pichard V, Briand C, Rognoni JB. Alpha2beta1-integrin signaling by itself controls G1/S transition in a human adenocarcinoma cell line (Caco-2): implication of NADPH oxidase-dependent production of ROS. Exp Cell Res 2003;285:59–71.
[16] Riganti C, Gazzano E, Polimeni M, Costamagna C, Bosia A, Ghigo D. Diphenyleneiodonium inhibits the cell redox metabolism and induces oxidative stress. J Biol Chem 2004;279:47726–31.
[17] Scaife RM. G2 cell cycle arrest, down-regulation of cyclin B, and induction of mitotic catastrophe by the flavoprotein inhibitor diphenyleneiodonium. Mol Cancer Ther 2004;3:1229–37.
[18] Block K, Gorin Y, Hoover P, Williams P, Chelmicki T, Clark RA, et al. NAD(P)H oxidases regulate HIF-2 alpha protein expression. J Biol Chem 2007;282:8019–26.
[19] Song JD, Kim KM, Kim KH, Kim CD, Kim JM, Yoo YH, et al. Differential role of diphenyleneiodonium, a flavoenzyme inhibitor, on p53-dependent and -independent cell cycle progression. Int J Oncol 2008;33:1299–306.

[20] Shoemaker RH. The NCI60 human tumour cell line anticancer drug screen. Nat Rev Cancer 2006;6:813–23.
[21] Paull KD, Shoemaker RH, Hodes L, Monks A, Scudiero DA, Rubinstein L, et al. Display and analysis of patterns of differential activity of drugs against human tumor cell lines: development of mean graph and COMPARE algorithm. J Natl Cancer Inst 1989;81:1088–92.
[22] Shoemaker RH, Monks A, Alley MC, Scudiero DA, Fine DL, McLemore TL, et al. Development of human tumor cell line panels for use in disease-oriented drug screening. Prog Clin Biol Res 1988;276:265–86.
[23] Holbeck SL, Collins JM, Doroshow JH. Analysis of Food and Drug Administration-approved anticancer agents in the NCI60 panel of human tumor cell lines. Mol Cancer Ther 2010;9:1451–60.
[24] Mukhopadhyay P, Rajesh M, Hasko G, Hawkins BJ, Madesh M, Pacher P. Simultaneous detection of apoptosis and mitochondrial superoxide production in live cells by flow cytometry and confocal microscopy. Nat Protoc 2007;2:2295–301.
[25] Downey T. Analysis of a multifactor microarray study using Partek genomics solution. Methods Enzymol 2006;411:256–70.
[26] Li N, Ragheb K, Lawler G, Sturgis J, Rajwa B, Melendez JA, et al. DPI induces mitochondrial superoxide-mediated apoptosis. Free Radic Biol Med 2003;34: 465–77.
[27] Doroshow JH, Gaur S, Matsumoto L, van Balgooy J, Markel S, Juhasz A. NADPH oxidase 1 (NOX1) inhibitors as novel therapeutic agents for colon cancer. Proc Am Assoc Cancer Res 2004;45:347.
[28] Pritsos CA, Keyes SR, Sartorelli AC. Effect of the superoxide dismutase inhibitor, diethyldithiocarbamate, on the cytotoxicity of mitomycin antibiotics. Cancer Biochem Biophys 1989;10:289–98.
[29] Doroshow JH. Anthracyclines and anthracenediones. In: Chabner BA, Longo DL, editors. Cancer chemotherapy and biotherapy: principles and practice. Philadelphia: Lippincott, Williams, and Wilkins; 2006. p. 414–50.
[30] Lambeth JD, Kawahara T, Diebold B. Regulation of Nox and Duox enzymatic activity and expression. Free Radic Biol Med 2007;43:319–31.
[31] Hutchinson DS, Csikasz RI, Yamamoto DL, Shabalina IG, Wikstrom P, Wilcke M, et al. Diphenylene iodonium stimulates glucose uptake in skeletal muscle cells through mitochondrial complex I inhibition and activation of AMP-activated protein kinase. Cell Signal 2007;19:1610–20.
[32] Coant N, Ben MS, Pedruzzi E, Guichard C, Treton X, Ducroc R, et al. NADPH oxidase 1 modulates WNT and NOTCH1 signaling to control the fate of proliferative progenitor cells in the colon. Mol Cell Biol 2010;30:2636–50.
[33] Yamaura M, Mitsushita J, Furuta S, Kiniwa Y, Ashida A, Goto Y, et al. NADPH oxidase 4 contributes to transformation phenotype of melanoma cells by regulating G(2)-M cell cycle progression. Cancer Res 2009;69:2647–54.
[34] Babior BM, Lambeth JD, Nauseef W. The neutrophil NADPH oxidase. Arch Biochem Biophys 2002;397:342–4.
[35] Mandal D, Fu P, Levine AD. REDOX regulation of IL-13 signaling in intestinal epithelial cells: usage of alternate pathways mediates distinct gene expression patterns. Cell Signal 2010;22:1485–94.
[36] Brand S, Beigel F, Olszak T, Zitzmann K, Eichhorst ST, Otte JM, et al. IL-22 is increased in active Crohn's disease and promotes proinflammatory gene expression and intestinal epithelial cell migration. Am J Physiol Gastrointest Liver Physiol 2006;290:G827–38.
[37] Pickert G, Neufert C, Leppkes M, Zheng Y, Wittkopf N, Warntjen M, et al. STAT3 links IL-22 signaling in intestinal epithelial cells to mucosal wound healing. J Exp Med 2009;206:1465–72.
[38] Hirakawa S, Saito R, Ohara H, Okuyama R, Aiba S. Dual oxidase 1 induced by Th2 cytokines promotes STAT6 phosphorylation via oxidative inactivation of protein tyrosine phosphatase 1B in human epidermal keratinocytes. J Immunol 2011;186:4762–70.
[39] Szatrowski TP, Nathan CF. Production of large amounts of hydrogen peroxide by human tumor cells. Cancer Res 1991;51:794–8.
[40] Gandara DR, Wiebe VJ, Perez EA, Makuch RW, DeGregorio MW. Cisplatin rescue therapy: experience with sodium thiosulfate, WR 2721, and diethyldithiocarbamate. Crit Rev Oncol Hematol 1990;10:353–65.
[41] Doroshow JH. Anthracycline antibiotic-stimulated superoxide, hydrogen peroxide, and hydroxyl radical production by NADH dehydrogenase. Cancer Res 1983;43:4543–51.
[42] Venkatachalam P, De Toledo SM, Pandey BN, Tephly LA, Carter AB, Little JB, et al. Regulation of normal cell cycle progression by flavin-containing oxidases. Oncogene 2008;27:20–31.
[43] Balcerczyk A, Soszynski M, Rybaczek D, Przygodzki T, Karowicz-Bilinska A, Maszewski J, et al. Induction of apoptosis and modulation of production of reactive oxygen species in human endothelial cells by diphenyleneiodonium. Biochem Pharmacol 2005;69:1263–73.
[44] Jiang F, Zhang Y, Dusting GJ. NADPH oxidase-mediated redox signaling: roles in cellular stress response, stress tolerance, and tissue repair. Pharmacol Rev 2011;63:218–42.
[45] Sharma P, Chakraborty R, Wang L, Min B, Tremblay ML, Kawahara T, et al. Redox regulation of interleukin-4 signaling. Immunity 2008;29:551–64.
[46] Simon AR, Rai U, Fanburg BL, Cochran BH. Activation of the JAK-STAT pathway by reactive oxygen species. Am J Physiol 1998;275:C1640–52.
[47] Simon AR, Takahashi S, Severgnini M, Fanburg BL, Cochran BH. Role of the JAK-STAT pathway in PDGF-stimulated proliferation of human airway smooth muscle cells. Am J Physiol Lung Cell Mol Physiol 2002;282:L1296–304.
[48] Meloche S, Pouyssegur J. The ERK 1/2 mitogen-activated protein kinase pathway as a master regulator of the G1-S-phase transition. Oncogene 2007;26:3227–39.
[49] Saunders JA, Rogers LC, Klomsiri C, Poole LB, Daniel LW. Reactive oxygen species mediate lysophosphatidic acid induced signaling in ovarian cancer cells. Free Radic Biol Med 2010;49:2058–67.
[50] Zhang Y, Kang YM, Tian C, Zeng Y, Jia LX, Ma X, et al. Overexpression of Nrdp1 in the heart exacerbates doxorubicin-induced cardiac dysfunction in mice. PLoS One 2011;6:e21104.
[51] Majander A, Finel M, Wikstrom M. Diphenyleneiodonium inhibits reduction of iron–sulfur clusters in the mitochondrial NADH-ubiquinone oxidoreductase (Complex I). J Biol Chem 1994;269:21037–42.